Available online at www.sciencedirect.com

SciVerse ScienceDirect

Ceramics International 39 (2013) 6743–6749

CERAMICS INTERNATIONAL

www.elsevier.com/locate/ceramint

Phase stability, microstructural and thermo-physical properties of $BaLn_2Ti_3O_{10}$ (Ln = Nd and Sm) ceramics

Lei Guo[a,b], Hongbo Guo[a,b,*], Guohui Ma[a], Shengkai Gong[a,b], Huibin Xu[a,b]

[a]School of Materials Science and Engineering, Beihang University, China

[b]Beijing Key Laboratory for Advanced Functional Material and Thin Film Technology, Beihang University, No. 37, Xueyuan Road, Beijing 100191, China

Received 6 January 2013; received in revised form 1 February 2013; accepted 2 February 2013
Available online 11 February 2013

Abstract

The phase stability, microstructural evaluation and thermo-physical properties of $BaLn_2Ti_3O_{10}$ (BLnT, Ln = Nd and Sm) ceramics for thermal barrier coating (TBCs) application have been investigated. BLnT (Ln = Nd and Sm) powders is found thermally stable at 1500 °C after exposure for 110 h, and the bulk materials exhibit lamellar structure. BLnT (Ln = Nd and Sm) bulk materials show anisotropy in thermo-physical properties due to the insertion of Ba atoms between [$Ln_2Ti_3O_{10}$] (Ln = Nd and Sm) sheets. The thermal conductivities of BLnT (Ln = Nd and Sm) are apparently lower than those of ZrO_2–8Y_2O_3 (8YSZ). Also, $BaSm_2Ti_3O_{10}$ exhibits relatively lower thermal conductivity as compared to $BaNd_2Ti_3O_{10}$. The thermal expansion coefficient (TEC) of BLnT (Ln = Nd and Sm) is found comparable to that of 8YSZ. $BaNd_2Ti_3O_{10}$ exhibits relatively larger TEC than $BaSm_2Ti_3O_{10}$. The above results suggest that BLnT (Ln = Nd and Sm) ceramics could be a good potential material for TBC applications.

Keywords: B. Microstructure-final; C. Thermal properties; E. Thermal applications; $BaLn_2Ti_3O_{10}$

1. Introduction

In advanced gas-turbines, thermal barrier coatings (TBCs) are required for improving the thermal efficiency and protecting hot components of gas turbines against high temperature and hot corrosion [1,2]. The TBCs system usually consists of a ceramic top coat, a metallic bond coat and Ni-based superalloy substrate. The state-of-the-art top coat material is 7–8 wt% Y_2O_3 stabilized ZrO_2 (YSZ). However, the problems of phase transformation and accelerated sintering limit the use of YSZ for operating above 1200 °C for long time [3,4]. At higher temperatures, metastable tetragonal phase decomposes into tetragonal and cubic phase. Upon cooling, the tetragonal phase transforms to monoclinic phase, giving rise to about 3.5% volume change and leading to crack formation in the TBCs. Furthermore, accelerated sintering occurs at high temperatures, which would decrease the volume fraction of pores, as a result would increase the thermal conductivity and restrict the favorable strain tolerance of the TBCs. Demand for enhanced jet engine efficiencies necessitates significant increase in combustion temperatures and operating pressures. To cope with these requirements, alternate TBCs materials are strongly required having lower thermal conductivity, higher temperature capability, and better sintering resistance at higher temperatures.

Extensive attention has been focused on different rare-earth doped zirconia [5,6], fluorite-structured materials [7,8], pyrochlore-structured materials [9–11], magnetoplumbite lanthanum hexaaluminate [12,13] and perovskite-structured materials [14]. Among these interesting candidate materials for TBC applications, the perovskites (ABO_3) are characterized by high melting point and low thermal conductivity. In perovskite-type ABO_3, the A ion is coordinated by twelve oxygen ions, whereas B ion is coordinated by six oxygen ions, forming BO_6 octahedra that share corners [15]. The most common type of distortion in perovskites is octahedral tilting. The perovskites consist of a class of crystal structures

*Corresponding author at: Beijing Key Laboratory for Advanced Functional Material and Thin Film Technology, Beihang University, No. 37, Xueyuan Road, Beijing 100191, China.
Tel./Fax: +86 10 8231 7117.
E-mail address: guo.hongbo@buaa.edu.cn (H. Guo).

0272-8842/$ - see front matter © 2013 Elsevier Ltd and Techna Group S.r.l. All rights reserved.
http://dx.doi.org/10.1016/j.ceramint.2013.02.003

that can accommodate a wide variety of different ions in solid solution, including ions with large atomic mass [2]. Several materials in this group, such as $BaZrO_3$ [3], $SrZrO_3$ [16], $CaZrO_3$ [17] and $SrHfO_3$ [18] were evaluated as TBCs candidate materials. Although the bulk properties of perovskites exhibit promising values, several problems, such as relatively lower toughness compared with YSZ, not sufficiently low thermal conductivity due to rigid structure and partial evaporation of constituents of the perovskite phase during coatings preparation were reported [2,19]. However, some hopeful developments in the area of perovskites are recent reports of several promising potential TBCs materials made of a layered perovskite with Ruddlesden–Popper structure.

In Ruddlesden–Popper structure, $A_2[A'_{n-1}B_nO_{3n+1}]$, the perovskite sheets, $[A'_{n-1}B_nO_{3n+1}]$, could be thought of as obtained by slicing the three-dimensional perovskite structure along one of the cubic directions [20]. $BaLn_2Ti_3O_{10}$ (Ln=lanthanide) crystallizes in the $n=3$ member of Ruddlesden–Popper structure, which contains alkaline earth cations, Ba, between perovskite sheets, $[Ln_2Ti_3O_{10}]$, as shown in Fig. 1 [21,22]. $BaLn_2Ti_3O_{10}$-type oxides with different Ln cations are of considerable scientific interest. $BaLa_2Ti_3O_{10}$ (BLT) bulk material produced by hot pressing was found to possess good phase stability at 1500 °C for 110 h, low thermal conductivity and large thermal expansion coefficient [21]. In our previous work, BLT coatings with nearly stoichiometric composition has been successfully produced by plasma spray, as seen in Ref. [23], and the coatings exhibit lower thermal conductivity and better thermal cycling performance compared to 8YSZ. BLT has been proposed as a promising TBCs material. As the typical members of $BaLn_2Ti_3O_{10}$ series, $BaNd_2Ti_3O_{10}$ and $BaSm_2Ti_3O_{10}$ are considered to have excellent phase stability and desirable thermo-physical properties for TBCs application.

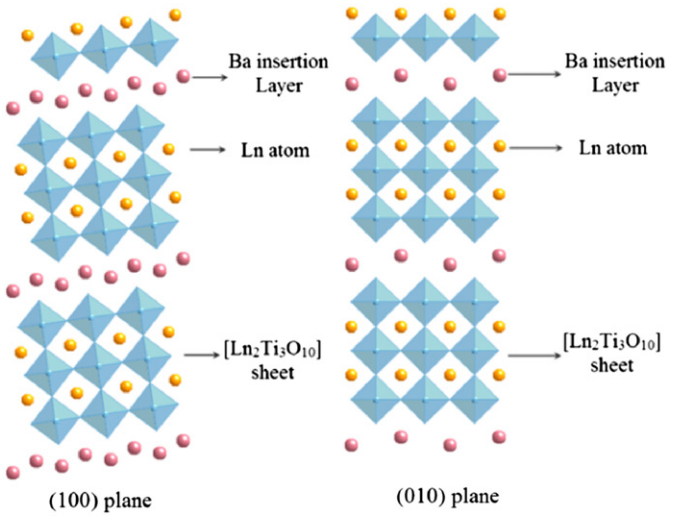

Fig. 1. $BaLn_2Ti_3O_{10}$ (Ln=Nd and Sm) crystal structure model on (100) plane and (010) plane showing $[Ln_2Ti_3O_{10}]$ sheets separated by Ba atoms.

The $BaNd_2Ti_3O_{10}$ and $BaSm_2Ti_3O_{10}$ ceramics for TBCs application have not been investigated so far in detail. In this research, the $BaNd_2Ti_3O_{10}$ and $BaSm_2Ti_3O_{10}$ powders were prepared by solid reaction method. The phase stability, structural and thermo-physical properties of $BaLn_2Ti_3O_{10}$ (BLnT, Ln=Nd and Sm) were studied in detail.

2. Experimental procedures

$BaLn_2Ti_3O_{10}$ (BLnT, Ln=Nd and Sm) powders were synthesized by solid state reaction method. The corresponding rare-earth oxides, Ln_2O_3 (Ln=Nd and Sm), $BaCO_3$ and TiO_2 (purity higher than 99.99%) were used as raw materials. The oxides powders were pre-calcined at 900 °C for 4 h to remove adsorptive water and/or carbon dioxide in air before weighting. The appropriate amounts of individual oxides were dissolved in ionized water and mechanically milled for 1 h, followed by drying at 160 °C overnight. The powders obtained after milling were calcined at 1500 °C for 8 h. The resultant powders were grinded and sieved with 450 μm screen.

$BaLn_2Ti_3O_{10}$ (Ln=Nd and Sm) powders were hot pressed at 1200 °C with a pressure of 20 MPa for 2 h and then annealed at 1500 °C to obtain bulk materials, which were used for the structural characterization and the evaluation of thermo-physical properties.

Phase composition analysis was carried out by X-ray diffraction (XRD, Rigaku Diffractometer, CuKα radiation). Scanning electron microscope (SEM, FEI, Holland) equipped with energy dispersive spectroscopy (EDS, IE 350) was used to observe the microstructure of the thermally etched cross-sections of bulk materials. The samples with cross-sections parallel and normal to hot pressing direction were prepared. SEM specimens were polished by routine metallographic techniques and then thermally etched at 1500 °C for 30 min in air.

Thermal diffusivity (λ) was measured using a laser flash device (NetzschLFA427, Germany). The specimens for thermal diffusivity measurement were cut into small disks with a diameter 12.7 mm and height 1 mm. BLnT (Ln=Nd and Sm) specimens with testing direction parallel and normal to hot pressing direction were denoted as BLnT1 and BLnT2, respectively. Both top and bottom of specimens were coated with a thin layer of graphite for thermal absorption of laser pulses. The thermal diffusivities of all specimens were measured three times at each temperature. The specific heat capacity (Cp) as a function of temperature was calculated from the chemical composition of BLnT (Ln=Nd and Sm) according to Neumann–Kopp rule. The heat-capacity data of the constituent oxides (Ln_2O_3, $BaCO_3$ and TiO_2) was obtained from the literature [24]. The bulk density (ρ) was measured by the Archimedes method, and the theoretical density (ρ_0) was calculated using lattice parameters acquired from XRD results and the molecular weight in a unit cell. The thermal

conductivity (κ) was calculated by the following equation

$$\kappa = \lambda C_p \rho \quad (1)$$

Because the sintered samples were not completely dense, the measured values of thermal conductivity (κ) was corrected for the actual data (κ_0) using the following equations

$$\frac{\kappa}{\kappa_0} = 1 - \frac{4}{3}\varphi \quad (2)$$

and

$$\varphi = 1 - \frac{\rho}{\rho_0} \quad (3)$$

where φ is the fractional porosity.

Thermal expansion coefficients (TECs) of samples were determined with a high-temperature dilatometer (Netzsch DIL 402E, Germany). Specimens used for TECs measurements were fabricated to the dimensions 4 mm × 4 mm × 25 mm. The TECs of BLnT (Ln = Nd and Sm) in longitudinal direction normal to hot pressing direction (BLnT3) and parallel to hot pressing direction (BLnT4) were both measured.

3. Results and discussion

3.1. Phase stability of $BaLn_2Ti_3O_{10}$

XRD analysis revealed that all the $BaLn_2Ti_3O_{10}$ (BLnT, Ln = Nd and Sm) powders synthesized in this study are basically composed of monoclinic phase as shown in Fig. 2a and b. High temperature XRD measurements (100–1100 °C) were carried out to evaluate the phase stability of BLnT (Ln = Nd and Sm) powders, the results are also included in Fig. 2. For both $BaNd_2Ti_3O_{10}$ and $BaSm_2Ti_3O_{10}$ powders, a slight shift in the diffraction peaks has been observed toward low angles with the increase in temperature due to thermal expansion of crystal lattice. It is important to note that peaks of BLnT (Ln = Nd and Sm) powders are almost unchanged, which indicates that no phase transformation occurred during high temperature XRD measurements. The influence of heat treatment on the phase constitution of $BaNd_2Ti_3O_{10}$ and $BaSm_2Ti_3O_{10}$ powders is presented in Fig. 2. After heat treatment at 1500 °C for 110 h, no phase transformation has been observed in both $BaNd_2Ti_3O_{10}$ and $BaSm_2Ti_3O_{10}$, which is indicative of their good phase stability. The good phase stability of BLnT (Ln = Nd, Sm) materials from room temperature to 1500 °C makes them to be the materials of choice for the applications as TBCs.

3.2. Structural characterization

Fig. 3 shows the thermally etched cross-sectional SEM micrographs of BLnT (Ln = Nd and Sm) bulk materials after heat treatment at 1500 °C for 1 h. In the section planes normal to the hot pressing direction, the grains of

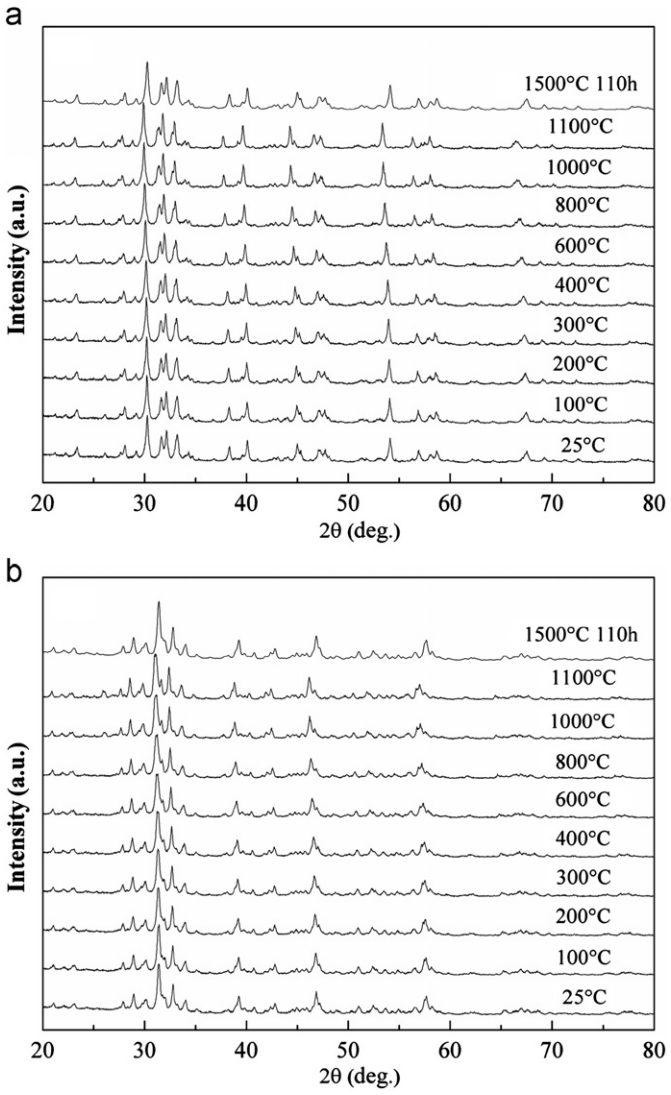

Fig. 2. XRD patterns of $BaLn_2Ti_3O_{10}$ (Ln = Nd and Sm) powders at elevated temperatures and after annealing at 1500 °C for 110 h: (a) $BaNd_2Ti_3O_{10}$; (b) $BaSm_2Ti_3O_{10}$.

$BaLn_2Ti_3O_{10}$ (Ln = Nd and Sm) exhibit plate-shaped appearance, as shown in Fig. 3a and c, while in section planes parallel to the hot pressing direction, the grains of BLnT (Ln = Nd and Sm) exhibit rod-shaped appearance, as shown in Fig. 3b and d. According to the cross-sectional micrograph from two perpendicular directions, it can be speculated that the grains of BLnT (Ln = Nd, Sm) exhibit lamellar structure. It has been reported that $BaLa_2Ti_3O_{10}$ bulk material prepared by hot pressing exhibits lamellar structure with *c*-axis texture and has anisotropic thermophysical properties [21]. Being the members of $BaLn_2Ti_3O_{10}$ series, it is reasonable to consider $BaSm_2Ti_3O_{10}$ and $BaNd_2Ti_3O_{10}$ bulk materials having similar structure and properties as those of $BaLa_2Ti_3O_{10}$ bulk material. The grain size distribution of $BaSm_2Ti_3O_{10}$ has been found to be more homogeneous than that of $BaNd_2Ti_3O_{10}$. The maximum grain size values of $BaNd_2Ti_3O_{10}$ and $BaSm_2Ti_3O_{10}$ are up to 25 μm and 30 μm, respectively.

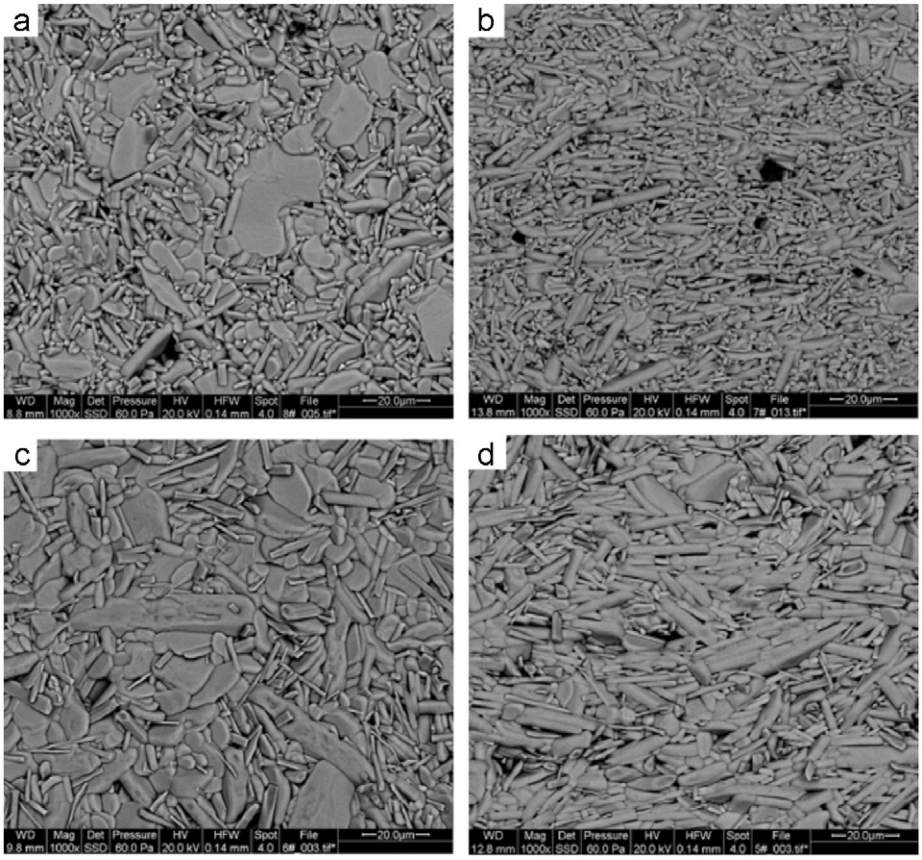

Fig. 3. SEM micrographs of $BaNd_2Ti_3O_{10}$ (a and b) and $BaNd_2Ti_3O_{10}$ (c and d) bulk materials after heat treatment at 1500 °C for 1 h: (a) and (c) section planes. normal to hot pressing direction; (b) and (d) section planes parallel to hot pressing direction.

Fig. 4 shows the SEM micrographs of section planes parallel to the hot pressing direction for BLnT (Ln = Nd and Sm) bulk materials sintered at 1500 °C for 110 h.

Compared with the samples sintered at 1500 °C for 1 h, no appreciable grain growth has been observed even after 110 h heat treatment at 1500 °C, which indicates that both $BaNd_2Ti_3O_{10}$ and $BaSm_2Ti_3O_{10}$ exhibit good resistance against sintering. As it is known, 8YSZ sinters easily above 1200 °C, it has been reported that the shrinkage of 8YSZ reach to about 0.056% after 10 h sintering at 1300 °C [6]. Compared to 8YSZ, BLnT (Ln = Nd, Sm) do not exhibit apparent sintering even after exposure to 1500 °C for 110 h as has been observed in the present study. After sintering at 1500 °C for 110 h, grain boundaries of $BaNd_2Ti_3O_{10}$ bulk material are clearly visible (Fig. 4a), while the grain boundaries of $BaSm_2Ti_3O_{10}$ bulk material have become a little blurry however, each grain can still be easily distinguished (Fig. 4b), which indicates that $BaNd_2Ti_3O_{10}$ exhibits better sintering resistance than $BaSm_2Ti_3O_{10}$. Good sintering resistance is one of criteria for the candidate materials for TBC applications.

3.3. Thermo-physical properties of $BaLn_2Ti_3O_{10}$

Fig. 5 shows the thermal diffusivities of BLnT1 and BLnT2 (Ln = Nd and Sm). Both $BaNd_2Ti_3O_{10}$ and $BaSm_2Ti_3O_{10}$ bulk materials exhibit anisotropy in thermal diffusivity. During the thermal diffusivity measurements, when the heat propagation direction was parallel to hot pressing direction (BNdT1 and BSmT1), the thermal diffusivities of $BaNd_2Ti_3O_{10}$ and $BaSm_2Ti_3O_{10}$ are in the ranges of 0.46–0.62 mm^2/s and 0.38–0.5 mm^2/s respectively. When the heat propagation direction was normal to hot pressing direction (BNdT2 and BSmT2), the thermal diffusivities of $BaNd_2Ti_3O_{10}$ and $BaSm_2Ti_3O_{10}$ are in the ranges of 0.56–0.7 mm^2/s and 0.46–0.56 mm^2/s, respectively. The anisotropy in thermal diffusivities of BLnT (Ln = Nd, Sm) bulk materials can be attributed to the insertion of Ba atoms between $[Ln_2Ti_3O_{10}]$ sheets in the crystal lattice, which is the same as for $BaLa_2Ti_3O_{10}$ bulk material reported in the literature [21].

The density measured by Archimedes method and the theoretical density calculated using lattice parameters acquired from XRD results are shown in Table 1. After sintering at 1500 °C for 1 h, the relative densities of $BaNd_2Ti_3O_{10}$ and $BaSm_2Ti_3O_{10}$ bulk materials reached 95% and 97%, respectively, which suggests that $BaNd_2Ti_3O_{10}$ exhibits a little better sintering resistance than $BaSm_2Ti_3O_{10}$. The specific heat capacity calculated according to Neumann–Kopp rule is shown in Table 2. The values of the thermal conductivity of BLnT1 and BLnT2 (Ln = Nd, Sm) bulk material can then be obtained using

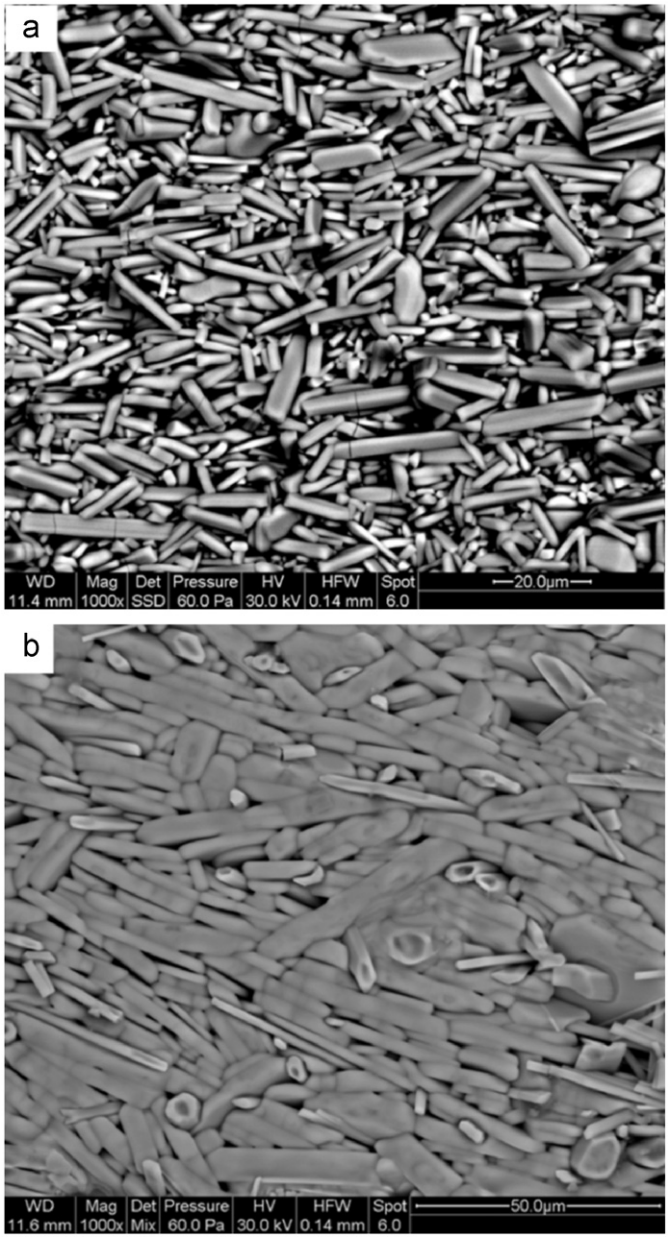

Fig. 4. SEM micrographs of $BaLn_2Ti_3O_{10}$ (Ln=Nd and Sm) bulk materials with. section planes parallel to hot pressing direction: (a) $BaNd_2Ti_3O_{10}$; (b) $BaSm_2Ti_3O_{10}$.

Eq. 1. The results after adjusting with Eq. 2 are plotted in Fig. 6. It can be found that $BaSm_2Ti_3O_{10}$ exhibits lower thermal conductivity than $BaNd_2Ti_3O_{10}$. For both $BaNd_2Ti_3O_{10}$ and $BaSm_2Ti_3O_{10}$, the thermal conductivities first decrease with the increase of the temperature below 300 °C, and then they increase above 300 °C, which may be attributed to the radiative transport in the thermal flash test. It can be seen from Fig. 6 that both $BaNd_2Ti_3O_{10}$ and $BaSm_2Ti_3O_{10}$ bulk materials exhibit anisotropy in thermal conductivity. The thermal conductivities of BNdT1 and BNdT2 are in the ranges of 1.5–2 W/mK and 1.8–2.4 W/mK, respectively, while those of BSmT1 and BSmT2 are in the ranges of 1.26–1.7 W/mK and 1.52–2.14 W/mK, respectively. The thermal conductivity of fully dense 8YSZ is

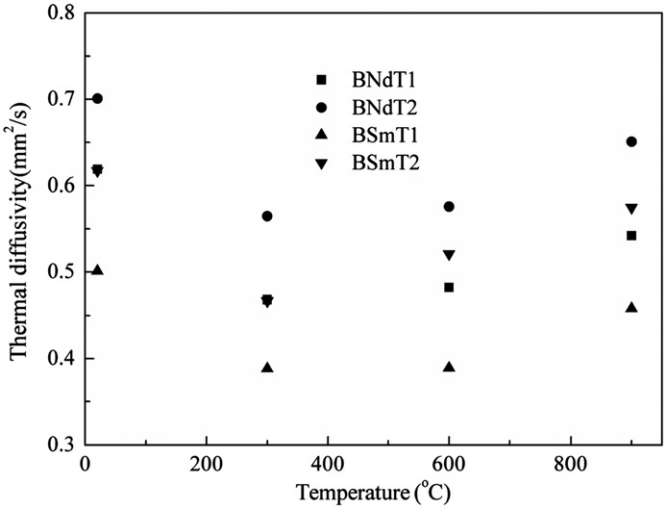

Fig. 5. Thermal diffusivities of $BaLn_2Ti_3O_{10}$ (Ln=Nd and Sm).

Table 1
Densities and theoretical densities of $BaLn_2Ti_3O_{10}$ (Ln=Nd and Sm) bulk materials.

Properties	$BaNd_2Ti_3O_{10}$	$BaSm_2Ti_3O_{10}$
Density (g/cm^3)	5.57	5.76
Theoretical density (g/cm^3)	5.86	5.94
Relative density (%)	95	97

Table 2
The specific heat capacity values of $BaLn_2Ti_3O_{10}$ (Ln=Nd and Sm) (J/(kg)).

Bulk materials	20 °C	300 °C	600 °C	900 °C
$BaNd_2Ti_3O_{10}$	0.463	0.546	0.592	0.629
$BaSm_2Ti_3O_{10}$	0.629	0.544	0.587	0.587

~2.2 W/mK [6]. The thermal conductivities of BLnT (Ln=Nd, Sm) are lower than those of 8YSZ, especially for BLnT2 bulk materials. The low thermal conductivities of BLnT (Ln=Nd and Sm) are beneficial to improve the thermal insulation property when applied on superalloy components such as blades, vanes and combustors.

The thermal expansion coefficients (TECs) of BLnT (Ln=Nd and Sm) bulk materials in the temperature range from 200 to 1200 °C are shown in Fig. 7, and the TEC of 8YSZ is included for comparison. It can be found from Fig. 7 that BLnT (Ln=Nd and Sm) exhibit anisotropy in TECs. The TECs of BNdT3 and BNdT4 are in the ranges of $9.4–11.4\times10^{-6}\,K^{-1}$ and $10.1–12.1\times10^{-6}\,K^{-1}$ respectively, while those of BSmT3 and BSmT4 are in the ranges of $9.5–10.5\times10^{-6}\,K^{-1}$ and $10–11.7\times10^{-6}\,K^{-1}$ respectively. The anisotropy in TECs of $BaNd_2Ti_3O_{10}$ and $BaSm_2Ti_3O_{10}$ bulk materials could be attributed to the insertion of Ba atoms between $[Ln_2Ti_3O_{10}]$ (Ln=Nd, Sm)

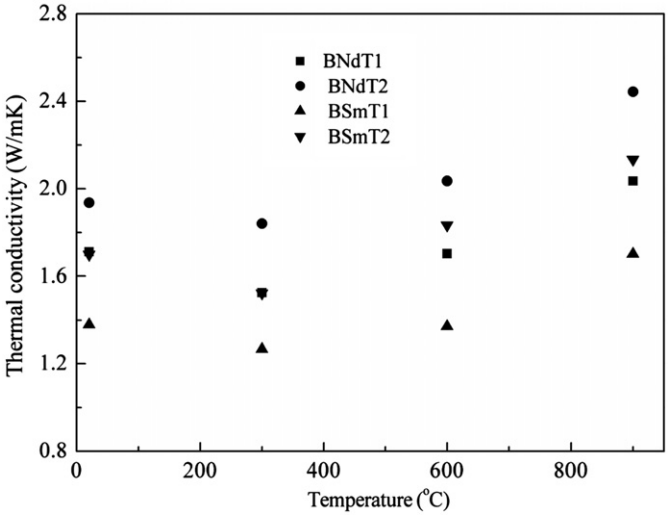

Fig. 6. Thermal conductivities of $BaLn_2Ti_3O_{10}$ (Ln = Nd and Sm).

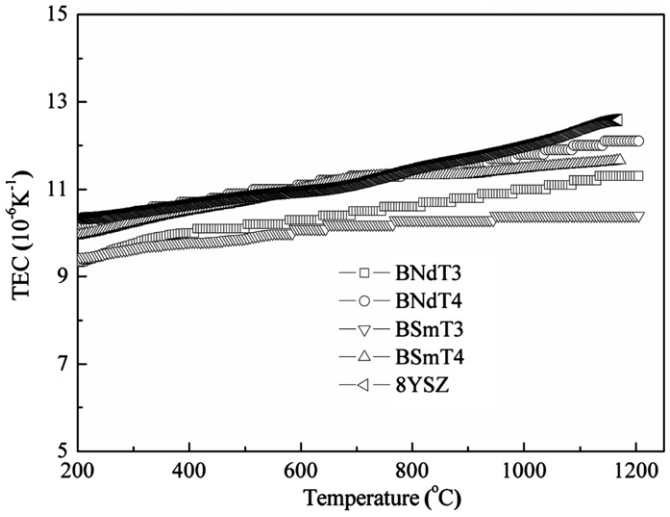

Fig. 7. Thermal expansion coefficients of $BaLn_2Ti_3O_{10}$ (Ln = Nd and Sm) and 8YSZ.

sheets, which is the same as for $BaLa_2Ti_3O_{10}$ reported in literature [21]. The TECs of BNT4 and BST4 are close to those of 8YSZ, which is beneficial to reduce the residual stress resulting from thermal expansion mismatch between coatings and superalloy substrate.

4. Conclusions

$BaLn_2Ti_3O_{10}$ (BLnT, Ln = Nd and Sm) ceramics were produced by solid state reaction.

Phase stability, microstructural evolution and thermophysical properties of BLnT (Ln = Nd and Sm) were investigated. Some conclusion can be drawn as follows:

(1) BLnT (Ln = Nd and Sm) powders exhibit phase stability after heat-treatment at 1500 °C for 110 h, and the bulk materials have lamellar structure. BLnT (Ln = Nd and Sm) bulk materials showed anisotropic thermophysical properties due to the insertion Ba atoms between $[Ln_2Ti_3O_{10}]$ (Ln = Nd and Sm) sheets.

(2) The thermal conductivities of $BaSm_2Ti_3O_{10}$ and $BaNd_2Ti_3O_{10}$ along hot pressing directions are in the ranges of 1.3–1.7 W/mK and 1.5–2 W/mK, respectively, apparently lower than those of 8YSZ. The TECs of $BaNd_2Ti_3O_{10}$ and $BaSm_2Ti_3O_{10}$ normal to hot pressing direction are in the ranges of $10.1–12.1 \times 10^{-6}\,K^{-1}$ and $10–11.7 \times 10^{-6}\,K^{-1}$, respectively, which are comparable to those of 8YSZ.

(3) The high temperature capability, low thermal conductivity and large thermal expansion coefficient of BLnT (Ln = Nd, Sm) ceramics suggest them as good potential materials for TBC applications. Our future work is directed to produce anisotropic BLnT (Ln = Nd and Sm) coatings aiming to exploit its comparative advantages in TBC applications.

Acknowledgments

This research is sponsored by Nature Science Foundations of China (NSFC) under Grant nos. 51071013 and 51231001, National Basic Research Program (973 Program) of China under Grant no. 2012CB625100.

References

[1] G.W. Goward, Progress in coatings for gas turbine airfoils, Surface and Coatings Technology 108–109 (1998) 73–79.
[2] R. Vassen, M.O. Jarligo, T. Steink, D.E. Mack, D. Stover, Overview on advanced thermal barrier coatings, Surface and Coatings Technology 205 (2010) 938–942.
[3] X.Q. Cao, R. Vassen, D. Stover, Ceramic materials for thermal barrier coatings, Journal of the European Ceramic Society 24 (2004) 1–10.
[4] A. Cipitria, I.O. Golosnoy, T.W. Clyne, A sintering model for plasma-sprayed zirconia TBCs. Part I: free-standing coatings, Acta Materialia 57 (2009) 980–992.
[5] Z.G. Liu, J.H. Ouyang, Y. Zhou, Effect of gadolinia on phase structure and thermal conductivity of ZrO_2–4.5 mol% Y_2O_3 ceramics, Materials Letters 62 (2008) 3524–3526.
[6] Y.L. Zhang, L. Guo, Y.P. Yang, H.B. Guo, H.J. Zhang, S.K. Gong, Influence of Gd_2O_3 and Yb_2O_3 Co-doping on phase stability, thermo-physical properties and sintering of 8YSZ, Chinese Journal of Aeronautics 25 (2012) 948–953.
[7] Y. Wang, H.B. Guo, S.K. Gong, Thermal shock resistance and mechanical properties of $La_2Ce_2O_7$ thermal barrier coatings with segmented structure, Ceramics International 35 (2009) 2639–2644.
[8] Z.H. Xu, L.M. He, Z.H. Tang, R.D. Mu, X.Q. Cao, Evolution of high temperature corrosion behavior of $La_2(Zr_{0.7}Ce_{0.3})_2O_7$ with the addition of Y_2O_3 thermal barrier coatings in contacts with vanadate-sulfate salts, Journal of Alloys and Compounds 536 (2012) 106–112.
[9] Z.G. Liu, J.H. Ouyang, B.H. Wang, Y. Zhou, J. Li, Thermal expansion and therma conductivity of $Sm_xZr_{1-x}O_{2-x/2}$ ($0.1 \le x \le 0.5$) ceramics, Ceramics International 35 (2009) 791–796.
[10] Z.G. Liu, J.H. Ouyang, Y. Zhou, X.L. Xia, Preparation and microstructural of $(Nd_{1-x}Gd_x)_2(Ce_{1-x}Zr_x)_2O_7$ solid solutions, Ceramics International 35 (2009) 2387–2392.
[11] C.L. Wan, Z.X. Qu, A.B. Du, W. Pan, Influence of B site substituent Ti on the structure and thermophysical properties of $A_2B_2O_7$-type pyrochlore $Gd_2Zr_2O_7$, Acta Materialia 57 (2009) 4782–4789.

[12] X.Y. Xie, H.B. Guo, S.K. Gong, H.B. Xu, Lanthanum-titanium-aluminum oxide: a novel thermal barrier coating material for applications at 1300 degrees C, Journal of the European Ceramic Society 31 (2011) 1677–1683.
[13] X.Q. Cao, Y.F. Zhang, J.F. Zhang, X.H. Zhong, Y. Wang, H.M. Ma, Z.H. Xu, L.M. He, F. Lu, Failure of the plasma-sprayed coating of lanthanum hexaluminate, Journal of the European Ceramic Society 28 (2008) 1979–1986.
[14] W. Ma, D.E. Mack, R. Vassen, D. Stove, Perovskite-type strontium zirconate as a new material for thermal barrier coatings, Journal of the American Ceramic Society 91 (2008) 2630–2635.
[15] C.J. Howard, H.T. Stokes, Structures and phase transitions in perovskites—a group-theoretical approach, Acta Crystallographica A 61 (2005) 93–111.
[16] W. Ma, D. Mack, J. Malzbender, R. Vassen, D. Stover, Yb_2O_3 and Gd_2O_3 doped strontium zirconate for thermal barrier coatings, Journal of the European Ceramic Society 28 (2008) 3071–3081.
[17] M.P. Srirama, M.V. Krishnaiah, Investigation of the thermal conductivity of calcium cerate and calcium zirconate, Materials Chemistry and Physics 31 (1992) 347–350.
[18] S. Yamanaka, T. Maekawa, H. Muta, T. Matsuda, S. Kobayashi, K. Kurosaki, Thermal and mechanical properties of $SrHfO_3$, Journal of Alloys and Compounds 381 (2004) 295–300.
[19] D.R. Clarke, S.R. Phillpot, Thermal barrier coating materials, Materials Today 8 (2005) 22–29.
[20] J. Gopalakrishnan, T. Sivakuma, K. Ramesha, V. Thangadurai, G.N. Subbanna, Transformations of Ruddlesden–Popper oxides to new layered perovskite oxides by metathesis reactions, Journal of the American Chemical Society 122 (2000) 6237–6241.
[21] L. Guo, H.B. Guo, G.H. Ma, M. Abbas, S.K. Gong, Ruddlesden–Popper structured $BaLa_2Ti_3O_{10}$, a highly anisotropic material for thermal barrier coatings, Ceramics International 38 (2012) 4345–4352.
[22] S. Sambasivan, K. Steiner, Highly Anisotropic Ceramic Thermal Barrier Coating Material and Related Composites, Patent no. US 6680126 B1, 2004.
[23] H.B. Guo, H.J. Zhang, G.H. Ma, S.K. Gong, Thermo-physical and thermal cycling properties of plasma-sprayed $BaLa_2Ti_3O_{10}$ coating as potential thermal barrier materials, Surface and Coatings Technology 204 (2009) 691–696.
[24] K.D. Maglic, A. Cezairliyan, V.E. Peletsky, Metallurgical Thermochemistry, Pergamon Press, London, 1976.